Local Treatment of a Pediatric Osteosarcoma Model with a 4-1BBL Armed Oncolytic Adenovirus Results in an Antitumor Effect and Leads to Immune Memory

Naiara Martinez-Velez[1,2,3], Virginia Laspidea[1,2,3], Marta Zalacain[1,2,3], Sara Labiano[1,2,3], Marc García-Moure[1,2,3], Montse Puigdelloses[1,2,4], Lucía Marrodan[1,2,3], Marisol Gonzalez-Huarriz[1,2,3], Guillermo Herrador[1,2,3], Daniel de la Nava[1,2,3], Iker Ausejo-Mauleon[1,2,3], Juan Fueyo[5], Candelaria Gomez-Manzano[5], Ana Patiño-García[1,2,3], and Marta M. Alonso[1,2,3]

ABSTRACT

Osteosarcoma is an aggressive bone tumor occurring primarily in pediatric patients. Despite years of intensive research, the outcomes of patients with metastatic disease or those who do not respond to therapy have remained poor and have not changed in the last 30 years. Oncolytic virotherapy is becoming a reality to treat local and metastatic tumors while maintaining a favorable safety profile. Delta-24-ACT is a replicative oncolytic adenovirus engineered to selectively target cancer cells and to potentiate immune responses through expression of the immune costimulatory ligand 4-1BB. This work aimed to assess the antisarcoma effect of Delta-24-ACT. MTS and replication assays were used to quantify the antitumor effects of Delta-24-ACT *in vitro* in osteosarcoma human and murine cell lines. Evaluation of the *in vivo* antitumor effect and immune response to Delta-24-ACT was performed in immunocompetent mice bearing the orthotopic K7M2 cell line. Immunophenotyping of the tumor microenvironment was characterized by immunohistochemistry and flow cytometry. *In vitro*, Delta-24-ACT killed osteosarcoma cells and triggered the production of danger signals. *In vivo*, local treatment with Delta-24-ACT led to antitumor effects against both the primary tumor and spontaneous metastases in a murine osteosarcoma model. Viral treatment was safe, with no noted toxicity. Delta-24-ACT significantly increased the median survival time of treated mice. Collectively, our data identify Delta-24-ACT administration as an effective and safe therapeutic strategy for patients with local and metastatic osteosarcoma. These results support clinical translation of this viral immunotherapy approach.

Introduction

Osteosarcoma is the most common primary bone tumor, affecting mainly children and adolescents, with a second minor peak of incidence at approximately 50 years of age (1). This malignant neoplasm is composed of mesenchymal cells that produce aberrant osteoid and immature bone, developing predominantly near the long bone metaphysis of limbs (2). The mainstay of current osteosarcoma treatment includes surgical resection of local and metastatic disease and pre- and postsurgical combination chemotherapy. The chemotherapy regimen includes a combination of doxorubicin and cisplatin with or without subsequent treatment with high-dose methotrexate and has a patient response rate of 70% (3). However, for patients with metastasis or recurrent disease, curative therapeutic options are limited, and the overall survival rate at 5 years is approximately 20%. This life expectancy is meager, underscoring the need for effective treatments, especially for high-risk populations.

Oncolytic virotherapy is a type of cancer biotherapy that has considered as a valid treatment option. Delta-24-RGD is a conditionally replicative adenovirus engineered to selectively replicate in cancer cells with an aberrant RB pathway (4, 5). In preclinical studies, Delta-24-RGD has shown efficacy in several solid adult (4, 6) and pediatric tumors, including local and metastatic osteosarcoma models (7–9). Clinically, Delta-24-RGD showed good safety and elicited a durable complete response in 20% of patients with recurrent glioblastoma (10). Importantly, the previous clinical trial revealed that intratumoral viral injection instigated an oncolytic effect followed by an inflammatory response potentially responsible for the antitumor effect and subsequent control of the tumor.

To further potentiate the efficacy of this virus, we engineered a new oncolytic virus expressing the immune costimulatory ligand 4-1BB (4-1BBL) to enhance viral antitumor immunity (11). 4-1BB is an inducible receptor promoting the survival and expansion of activated T cells. The interaction of 4-1BBL with 4-1BB enhances the stimulation of $CD4^+$ and $CD8^+$ T cells, causing predominant expansion of $CD8^+$ T cells (12). Signals initiated by 4-1BBL–4-1BB binding promote the $CD8^+$ T-cell costimulation, playing an important role in the differentiation of effector memory responses. Therefore, we hypothesized that the oncolytic adenovirus Delta-24-ACT

[1]Health Research Institute of Navarra (IDISNA), Pamplona, Navarra, Spain. [2]Program in Solid Tumors, Foundation for the Applied Medical Research, Pamplona, Navarra, Spain. [3]Department of Pediatrics, Clínica Universidad de Navarra, Pamplona, Spain. [4]Department of Neurology, Clínica Universidad de Navarra, Pamplona, Spain. [5]Department of NeuroOncology, The University of Texas MD Anderson Cancer Center, Houston, Texas.

Note: Supplementary data for this article are available at Molecular Cancer Therapeutics Online (http://mct.aacrjournals.org/).

N. Martinez-Velez, V. Laspidea, and M. Zalacain contributed equally to this article.

A. Patiño-García and M.M. Alonso contributed equally as the co-senior authors of this article.

Corresponding Authors: Ana Patiño-García, Dept. of Pediatrics, BTBT Lab, University Hospital of Navarra, University of Navarra, Pamplona, Spain. Phone: 349-4825-5400, ext. 4523; E-mail: apatigar@unav.es; and Marta M. Alonso, Phone: 349-4819-4700, ext. 812026; E-mail: mmalonso@unav.es

Mol Cancer Ther 2022;21:471–80

doi: 10.1158/1535-7163.MCT-21-0565

expressing 4-1BBL could trigger an immune response that would lead to a specific antisarcoma effect not only controlling local disease but also resulting in a therapeutic effect on distant untreated lung metastasis.

Materials and Methods

Cell lines and culture conditions

The murine osteosarcoma cell line K7M2 was obtained from the American Type Culture Collection (ATCC cat. No. CRL-2836, RRID: CVCL_V455). The murine osteosarcoma POS-1 and MOS-J cells derived from mouse spontaneous osteosarcoma were provided, respectively, by Drs. Kamijo (13) and Shultz (14) and were cultured in RPMI and DMEM, respectively with 10% FBS and 1% penicillin/streptomycin. The pediatric human osteosarcoma cell line Saos-2 was obtained from ATCC (cat. No. 300331/p651_SaOS-2, RRID: CVCL_0548). 531MII, a primary osteosarcoma cell line, was developed at the Clínica Universidad de Navarra. Cell lines obtained from ATCC were cultured following the manufacturer's instructions. 531MII cells were cultured in minimum essential medium supplemented with 10% FBS and 1% antibiotic. All cells were maintained in a humidified atmosphere with 5% CO_2 at 37°C. Cell lines were routinely tested for *Mycoplasma* (MycoAlert Mycoplasma Detection Kit; Lonza), and human cell lines were authenticated at the CIMA Genomic Core Facility.

Delta-24-ACT construction

Delta-24-ACT was constructed by maintaining the Delta-24-RGD modifications of a 24-base pair deletion and introduction of RGD (15); however, m4-1BBL was incorporated in the E3 locus after removing this gene. Briefly, murine 4-1BBL was first cloned into a pCDNA3.1 plasmid using the *Kpn I* and *Xho I* restriction enzymes (New England Biolabs). Then, m4-1BBL flanked with the cytomegalovirus promoter and bovine growth hormone polyadenylation sequences was subcloned into the pAB26-RGD plasmid at the *Cla I*/*BamH I* site. Finally, the 4-1BBL expression cassette was introduced into pVK-500C-Δ24, and the Delta-24 plasmid was constructed by homologous recombination with pAB26-m4-1BBL in BJ5183 bacteria. For viral rescue, the obtained plasmid was linearized with *Pac I* and transfected into HEK293 cells (cat. No. 300192/p777_HEK293, RRID:CVCL_0045) with Lipofectamine 2000 (Invitrogen). After confirmation of genetic modifications by PCR and sequencing, Delta-24-ACT was amplified in A549 cells (cat. No. 300114/p686_A-549, RRID:CVCL_0023), purified, and stored at −80°C.

Cell viability assay

All cell lines were seeded at a density of 10^3 cells per well in 96-well plates and infected with Delta-24-RGD and Delta-24-ACT at different multiplicity of infections ranging from 0 to 300. Cell viability was assessed 5 days after infection using a CellTiter 96 Aqueous One Solution Cell Proliferation Assay (Promega). The dose–response curves and IC_{50} values were analyzed using GraphPad software (RRID:SCR_002798 v8).

Replication assay

Cells were plated at a density of 5×10^4 and were then infected at an MOI of 10 for human cell lines and 300 for murine cell lines. Seventy-two hours later, the cells and supernatant were collected and subjected to three freeze-thaw cycles. The supernatant was used to infect HEK293 cells, and viral PFUs were determined by the anti-hexon staining method.

Infectivity assay

Cell lines were plated in 96-well plates at a density of 2×10^5 and infected at an MOI of 10 with a nonreplicative virus expressing GFP. After 24 hours, infected cells were harvested, and GFP expression was quantified by flow cytometry.

Immunoblotting

For immunoblotting, samples were subjected to SDS-Tris-Gly gel electrophoresis. Membranes were incubated with antibodies specific for the following molecules: E1A, (1:1,000; Santa Cruz Biotechnology cat. No. sc-430, RRID:AB_630843, Santa Cruz Biotechnology), fiber (1:1,000; Novus cat. No. NB 600–541, RRID:AB_521564, Novus Biological), GRB-2 (1:1,000; BD Biosciences cat. No. 610111, RRID:AB_397517), and LC3 A/B (1:1,000; Cell Signaling Technology cat. No. 4108, RRID:AB_213770).

Immunohistochemical analysis

Paraffin-embedded sections of mouse tibias, lungs, and livers were immunostained following conventional procedures with these antibodies: adenoviral mouse anti-hexon (Chemicon International, Inc.), adenovirus rabbit anti-E1A, (Santa Cruz Biotechnology), anti-CD3 (NeoMarkers), anti-CD4 (Abcam), anti-CD8a (Cell Signaling Technology), anti-FoxP3 (eBioscience, Thermo Fisher Scientific), and anti-vimentin clone V9 (IS30, Dako Denmark A/S). For immunohistochemical staining, Vectastain ABC Kits (Vector Laboratories Inc.) were used according to the manufacturer's instructions.

Measurement of DAMPs

Cell lines were plated and infected with both viruses at MOIs of 25 and 300, and medium was collected 72 hours later. ATP release was assessed with an ENLITEN ATP Assay System (FF2000, Promega). HMGB1 and HSP-90 release into the medium was measured with an HMGB1 ELISA Kit (ST51011, IBL International) and an HSP-90A ELISA kit (ADI-EKS-895, Enzo Life Sciences Inc.).

Calreticulin translocation to the plasma membrane was determined by immunofluorescence staining of 2×10^4 cells infected with Delta-24-ACT at a dose corresponding to the 3-day IC_{50} (or with PBS as a negative control). Four hours postinfection, cells were fixed with 4% methanol-free formaldehyde (28906; Thermo Fisher Scientific) for 15 minutes at 37°C and were then stained with appropriate antibodies.

Flow cytometric analysis

Viral 41BBL expression in osteosarcoma cell lines was determined by flow cytometry. Cells were stained first with a cell death detection antibody in the Zombie-NIR Fixable Viability Kit (423105, BioLegend) following the manufacturer's protocol and then with a PE-conjugated anti–4-1BBL antibody.

Calreticulin cell surface expression was determined by flow cytometry. Cells were stained first with a cell death detection antibody in the Zombie Green Fixable Viability Kit (423111, BioLegend) and then with a fluorophore-conjugated anti-calreticulin antibody (Abcam).

Fluorescence emission was analyzed using a FACSCanto II system with FACSDiva software (RRID:SCR_001456).

To identify immune cell populations, infiltrating immune cells were surface stained with the following antibody panel: anti–CD45-AF700 (BioLegend), anti–Ly6G-PerCP-Cy5.5 (BioLegend), anti–Ly6C-FITC (BioLegend), anti–F4/80-APC (BioLegend), anti–CD8-BV510 (BioLegend), anti–CD11b-BUV395 (BioLegend), and anti–CD4-BUV496 (BioLegend). PromoFLuor840 maleimide (PromoKine) was used as a viability marker. Samples were acquired with a CytoFlex flow

cytometer (Beckman Coulter RRID:SCR_019627) and data analyses were performed using FlowJo v10 (RRID:SCR_008520).

IFNγ and cytokine detection

Splenocytes and tumor-infiltrating lymphocytes (TILs) isolated from treated mice were cocultured with 10,000 K7M2 cells. K7M2 cells were left uninfected or infected with Delta-24-RGD or Delta-24-ACT at an MOI of 100 MOI. Four hours later, K7M2 cells were stimulated with recombinant mouse IFNγ protein and were collected and fixed with 4% formaldehyde 48 hours later. After 72 hours of coculture, supernatants were collected, and IFNγ ELISA (R&D Systems, Inc.) and MACS Plex Mouse Cytokine 10 kits (Miltenyi Biotec, Bergisch Gladbach) were used for analysis following the manufacturers' instructions.

Animal studies

The Ethical Committee of the University of Navarra [Comite Etico de Experimentacion Animal (CEEA)] approved the animal protocols performed in this study (CEEA/022–16). All animal studies were performed at the veterinary facilities of the Center for Applied Medical Research following institutional, regional, and national laws and ethical guidelines for experimental animal care.

To establish osteosarcoma animal models, K7M2 cells were injected into female BALB/c mice through the tibial plateau into the primary spongiosa of the right tibia. PBS or viruses (10^8 pfu/mouse) were administered intratumorally on days 10 and 18 after tumor engraftment. Tumor development and mouse weight were monitored twice weekly during the experiment. The tibia size was measured from the beginning of the experiment, and mice were sacrificed when the tumor volume reached 400 mm^2. Tumor volumes were determined throughout the course of the experiment by measuring the tumors along the two perpendicular diameters with a caliper and calculating the tumor volume with the following formula: volume $= D \times (d)^2 \times 0.5$, where D is the largest diameter and d is the smaller diameter. Animals were sacrificed when the tibial tumor volume reached 430 mm^3 or when they lost more than 20% of their body weight, and we harvested tibias to examine primary bone tumors, lungs to examine metastases, and livers to evaluate safety.

In vivo pulmonary metastasis evaluation

Thorax tomography was performed on mice anesthetized by intraperitoneal injection of ketamine and xylazine. Then, an intratracheal cannula was placed and connected to a flexiVent rodent ventilator (Scireq) set at a rate of 200 breaths/minute and a tidal volume of 10 mL/kg. Animals were maintained on 2% isoflurane inhalation until completely relaxed.

Lung 3D tomographic images were acquired using an X-ray micro-CT system (Quantum-GX, Perkin Elmer) with the following parameters: X-ray source voltage of 90 kVp, current of 88 μA, high-speed scan protocol for a total acquisition time of 14 minutes, and gantry rotation of 360°. Breathing artifacts were denoised using respiratory gating in each acquisition. The three-dimensional tomographic images containing the whole lung had a total of 512 slices with an isotropic voxel size of 72 μm and a resolution of 512 × 512 pixels per slice. Analysis of the lung volume in each sample was carried out using Fiji/ImageJ (RRID:SCR_002285), open-source Java-based image processing software. In brief, lung images were segmented by applying a fixed threshold, and total lung volume was measured over the obtained mask (mm^3). Quantified values were normalized to those of normal, healthy lung parenchyma.

Statistical analysis

The *in vitro* experiments were repeated at least three times. Dose–response curves for viral cytotoxicity were obtained by nonlinear regression. Data with normal distributions were assessed by Shapiro–Wilk tests, and comparisons among groups were performed by two-tailed nonparametric tests with 95% confidence intervals for nonnormally distributed datasets or parametric tests when normality was confirmed (Student t test or one/two-way ANOVA). For comparison of groups in survival experiments, a log-rank test (Mantel–Cox) was used. GraphPad Prism 8 (Statistical Software for Sciences GraphPad Prism) was used for the statistical analyses.

Results

The oncolytic adenovirus Delta-24-ACT is effective against osteosarcoma cells *in vitro*

Delta-24-ACT is a replicative oncolytic adenovirus based on the Delta-24-RGD (4) backbone and modified to encode the mouse 4-1BBL (m4-1BBL; Supplementary Fig. S1A). We showed that the 4-1BBL expressed by the virus was functional and effectively activated T cells *in vitro* and *in vivo* in the context of murine glioma models (15). Human pediatric osteosarcoma cells express receptors (αv3 and αv5 integrins and CAR) necessary for viral entry into cells (16), and Delta-24-ACT utilizes these receptors for recognition and subsequent entry into cells. Thus, we confirmed that Delta-24-ACT was able to infect 531MII and Saos-2 human osteosarcoma cells and K7M2 osteosarcoma cells (Supplementary Fig. S1B). Moreover, K7M2, 531 MII and Saos-2 cells infected with an increasing amount of virus showed dose-dependent expression of 4-1BBL mRNA that was efficiently translated to protein (**Fig. 1A** and **B**; Supplementary Fig. S1C). Importantly, we confirmed that after infection with Delta-24-ACT, 4-1BBL was expressed on the surface of murine (**Fig. 1C** and **D**; Supplementary Fig. S1D) and human osteosarcoma cells (**Fig. 1C**; Supplementary Fig. S1D).

Because viral genome modifications can interfere with effective viral replication, the replication capacity of Delta-24-ACT was quantified and compared with that of Delta-24-RGD in osteosarcoma cell lines after 72 hours of infection. No differences were found between the load of Delta-24-RGD and Delta-24-ACT progeny virions, indicating that insertion of the m4-1BBL expression cassette did not hinder viral replication (**Fig. 1E**; Supplementary Fig. S1E). Finally, the results of cytotoxicity tests showed that both Delta-24-RGD and Delta-24-ACT exerted a potent antitumor effect *in vitro* in all tested osteosarcoma cell lines (**Fig. 1F**; Supplementary Fig. S1F). We observed that both viruses displayed very similar IC_{50}s: Delta-24-RGD proved slightly better although not significant. In K7M2, the IC_{50s} were 27 ± 11.2 and 24 ± 7.9 MOIs for Delta-24-ACT and Delta-24-RGD, respectively. In 531MII were 10.1 ± 3.5 and 7.5 ± 2.4 MOIs for Delta-24-ACT and Delta-24-RGD, respectively. In addition, we confirmed the capability of Delta-24-ACT to replicate and to express m4-1BBL in osteosarcoma tumors *in vivo*. We detected m4-1BBL mRNA and protein expression in osteosarcoma tumors 48 hours after Delta-24-ACT treatment (**Fig. 1G** and **H**). We also observed the presence of viral proteins, specifically E1A and fiber in orthotopic osteosarcoma tumors treated with Delta-24-ACT (**Fig. 1H**). Importantly, the presence of the fiber protein, which is expressed in the late stages of the viral life cycle, suggested viral replication *in vivo*.

In summary, these results demonstrated that the newly generated virus Delta-24-ACT efficiently expressed m4-1BBL in osteosarcoma cells both *in vitro* and *in vivo*, indicating preservation of its replication capacity.

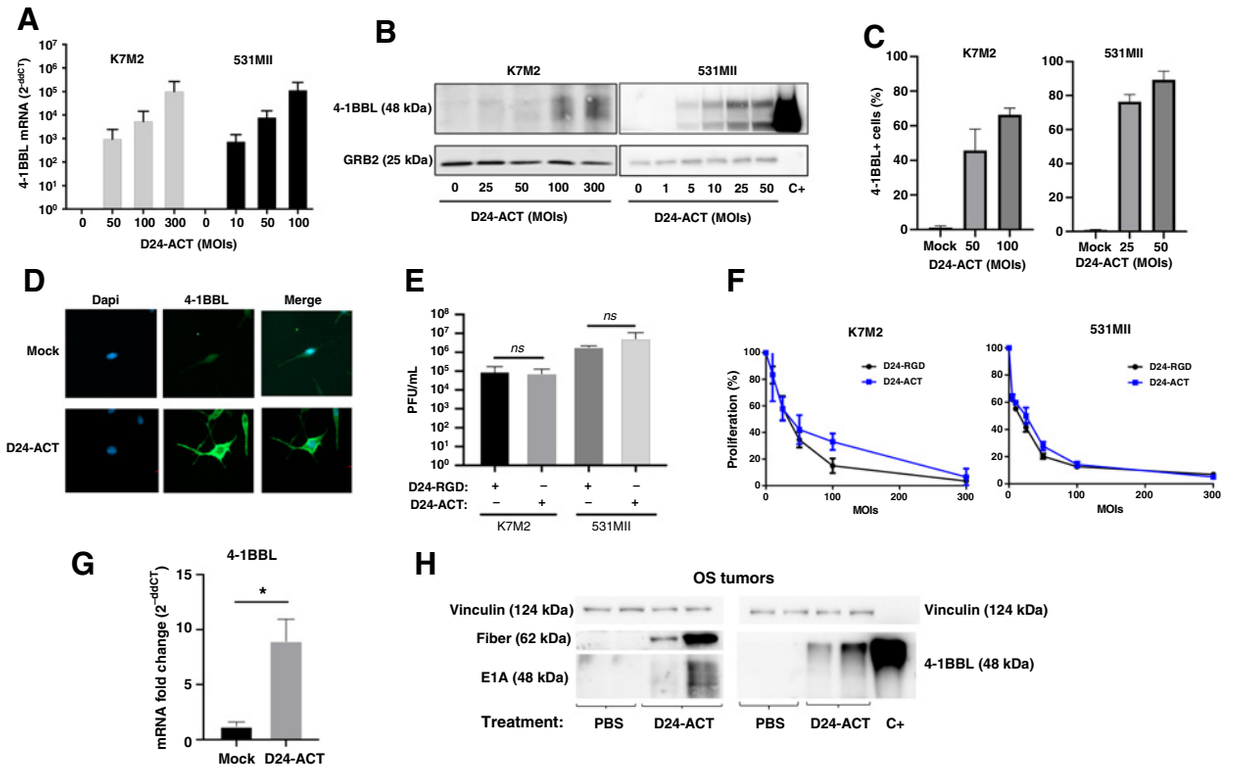

Figure 1.

Characterization of Delta-24-ACT in osteosarcoma cell lines. **A,** Expression of 4-1BBL mRNA after infection with Delta-24-ACT at the indicated MOIs in K7M2 and 531MII cells ($N = 3$). **B,** Assessment of 4-1BBL protein expression by Western blot analysis. Cells were infected with Delta-24-ACT at the indicated MOIs, and 48 hours later, whole-cell lysates were collected. Grb2 was used as the protein loading control, and recombinant 4-1BBL protein was used as the positive control. **C,** Flow cytometric quantification of 4-1BBL expression in the membrane of murine (K7M2) and human (531MII) osteosarcoma cells infected with Delta-24-ACT at the indicated MOIs. **D,** Representative fluorescence micrographs of K7M2 cells 24 hours after infection with Delta-24-ACT or mock infection. 4-1BBL at the cell surface was detected by immunofluorescence (green). Samples were counterstained with DAPI (blue). **E,** Replication of Delta-24-ACT in murine K7M2 and human 531MII osteosarcoma cells. Cells were infected, and Delta-24-ACT replication was determined after 72 hours. The results are expressed as the mean viral titers ± SDs ($N = 3$). **F,** Oncolytic effect of Delta-24-ACT and Delta-24-RGD on murine and human osteosarcoma cells. To quantify the oncolytic effect of the viruses, cells were infected at the indicated MOIs, and five days later, viability was evaluated by MTS assays. The values indicate the percentages of viable cells in infected cultures compared with those in noninfected cultures (mean ± SD). **G,** *In vivo* evaluation of 4-1BBL mRNA expression in orthotopic human osteosarcoma tumors**. H,** Assessment of 4-1BBL, E1A, and fiber expression *in vivo* in orthotopic human osteosarcoma tumors by Western blot analysis. A representative blot is shown.

Delta-24-ACT treatment *in vitro* leads to the production of DAMPs

Autophagy mediates the release of damage-associated molecular patterns (DAMPs) and tumor antigens; therefore, its stimulation has been proposed to be required for immunogenic cell death (ICD; refs. 17–20). Consequently, we assessed whether Delta-24-ACT treatment induces autophagy. We observed an increase in the conversion of LC3I to LC3II and a decrease in the P62/GRB2 ratio in Delta-24-ACT–infected cells compared with Delta-24-RGD–infected cells (Supplementary Fig. S2A). Next, we evaluated whether Delta-24-ACT–induced autophagy led to the release of several DAMPs by evaluating ATP, HMGB1, and HSP-90α release and calreticulin (CRT) exposure in the membrane as hallmarks of ICD. We observed an increase in ATP release in K7M2 ($P = 0.04$) and 531MII ($P = 0.03$) cells 72 hours after treatment with Delta-24-RGD or Delta-24-ACT (**Fig. 1A**). The level of HMGB1 release tended to increase, although nonsignificantly, in both cell lines after viral treatment (Supplementary Fig. S2B). In addition, HSP-90α release, a marker of ICD in human cells, was significantly increased in 531MII cells infected with either Delta-24-ACT or Delta-24-RGD compared with control cells (mock-infected; **Fig. 2B**). Moreover, calreticulin translocation from the endoplasmic reticulum to the cell membrane, forming clusters in K7M2 and 531MII cells after Delta-24-ACT infection, was observed (**Fig. 2C**; Supplementary Fig. S2C). Quantification of calreticulin expression in the membrane of K7MII and 531MII cells showed a significant increase in both cell lines infected with the either virus ($P = 0.002$ and $P = 0.02$ for K7MII cells and 531MII cells, respectively; **Fig. 2D**). In summary, Delta-24-ACT treatment of osteosarcoma cells triggered the production of several DAMPs *in vitro*.

Delta-24-ACT administration significantly stimulates immune infiltration and establishes a proinflammatory microenvironment in murine osteosarcoma tumors

Previously, we showed that Delta-24-RGD treatment triggered an immune response in glioma and DIPG models (7, 10, 21). In fact, viral administration induces the production of DAMPs that attract immune cell populations to the tumor site, eliciting a specific immune response against tumor cells (17). Therefore, BALB/c mice bearing K7M2 murine osteosarcoma cells orthotopically were treated twice with PBS,

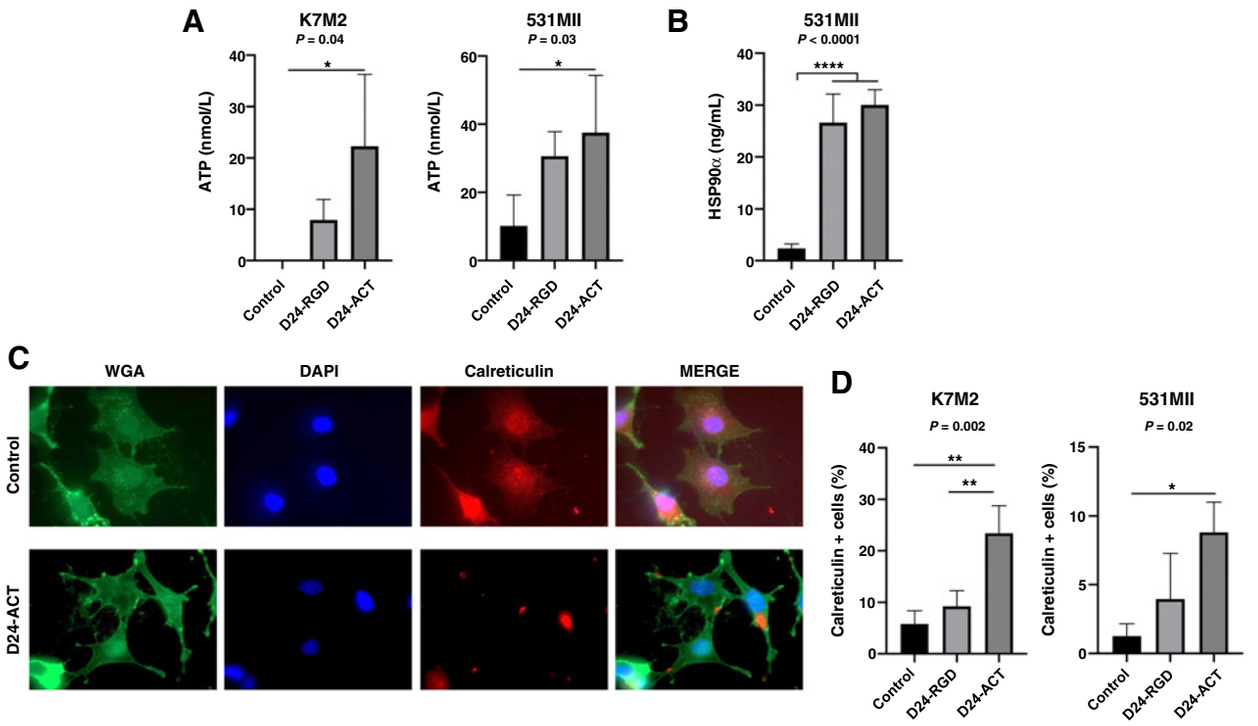

Figure 2.

Delta-24-ACT mediates DAMP release *in vitro*. **A** and **B,** Concentrations of the DAMPs ATP and Hsp90α in supernatants obtained from osteosarcoma cell cultures 72 hours after infection with Delta-24-ACT at the corresponding IC_{50} values for each virus or mock infection. The bar graphs show the mean ± SD values ($n = 3$; ordinary one-way ANOVA with Tukey multiple comparison test). **C,** Representative fluorescence micrographs of K7M2 cells 4 hours after infection with Delta-24-ACT or mock infection. Calreticulin at the cell surface was detected by immunofluorescence (red). Cell membranes (green) and nuclei (blue) were counterstained with wheat germ agglutinin (WGA) and DAPI, respectively. **D,** Flow cytometric quantification of membrane calreticulin + cells after Delta-24-ACT or Delta-24-RGD infection. The bar graphs show the mean ± SD values ($n = 3$; ordinary one-way ANOVA with Tukey multiple comparison test).

Delta-24-RGD, or Delta-24-ACT (days 10 and 18). Anatomopathological studies revealed a significant increase in infiltrating $CD3^+$ and $CD8^+$ cells in tumors treated with Delta-24-ACT compared with those treated with Delta-24-RGD ($P < 0.05$) or PBS ($P < 0.001$). The infiltration density was increased almost twofold in Delta-24-ACT–treated mice compared with Delta-24-RGD–treated mice (**Fig. 3A** and **B**). On the other hand, $CD4^+$ cells were increased in treated tumors, although the difference was not significant (Supplementary Fig. S3A). Quantification of several immune cell populations by flow cytometry at day 7 posttreatment (Supplementary Fig. S3B) confirmed that both viruses significantly increased the number of $CD45^+$, CD3, CD8, CD4, Trg, NK cells, macrophages, and DCs in the tumor (all $P < 0.05$). However, we did not find significant differences among both viruses (**Fig. 3C**). A second experiment confirmed that Delta-24-ACT increased the numbers of $CD3^+$ cells, $CD4^+$ cells, $CD8^+$ cells, and macrophages compared with those in PBS-treated mice ($P = 0.002$, $P = 0.03$, $P = 0.04$, and $P = 0.001$, respectively; **Fig. 3D**). Moreover, $CD4^+$ and $CD8^+$ cells tended to express higher levels of $CD137^+$ (**Fig. 3D**), suggesting that T-cell activation was increased. Quantification of IFNg production in splenocytes isolated from mice in the different treatment groups showed that compared with PBS, both viruses increased significantly the level of this cytokine measured by ELISA ($P = 0.01$ and $P < 0.001$ for Delta-24-RGD and Delta-24-ACT, respectively; **Fig. 3E**). Moreover, splenocytes from Delta-24-ACT–treated mice displayed a more active phenotype than those from Delta-24-RGD ($P = 0.02$). This finding was further confirmed by ELISPOT, which showed that the coculture of K7M2 cells with splenocytes from Delta-24-ACT–treated mice led to a nearly threefold increase in the production of IFNg as compared with the PBS group ($P < 0.0001$; **Fig. 3F**). Delta-24-ACT was also superior to Delta-24-RGD ($P = 0.006$). Moreover, intratumoral injection of Delta-24-ACT led to upregulation of proinflammatory cytokines such as IFNg, GM-CSF, IL5, and IL4 in the tumor. Interestingly, we did not observe any difference in the expression of IL2 or IL12. In addition, virus injection did not induce any changes in protumoral cytokines (Supplementary Fig. S3C).

Collectively, these results showed that Delta-24-ACT increased immune infiltration, inducing a proinflammatory microenvironment.

Delta-24-ACT local administration presents a safe toxicity profile

Because 4-1BB agonists have shown hepatic toxicity in clinical settings (reviewed in refs. 8, 22), we first evaluated the safety of intratumoral administration of Delta-24-ACT. Administration of one or three doses of virus did not affect the weight of the treated animals (**Fig. 4A**). Moreover, quantification of murine hepatic transaminases 48 hours after a single dose and after three doses of Delta-24-ACT revealed no differences in blood alanine aminotransferase (ALT) and aspartate aminotransferase (AST) levels (**Fig. 4B**), suggesting normal hepatic function. Histopathologic analysis confirmed that the livers from virus-treated animals were morphologically normal (**Fig. 4C**), indicating the safety of the virus.

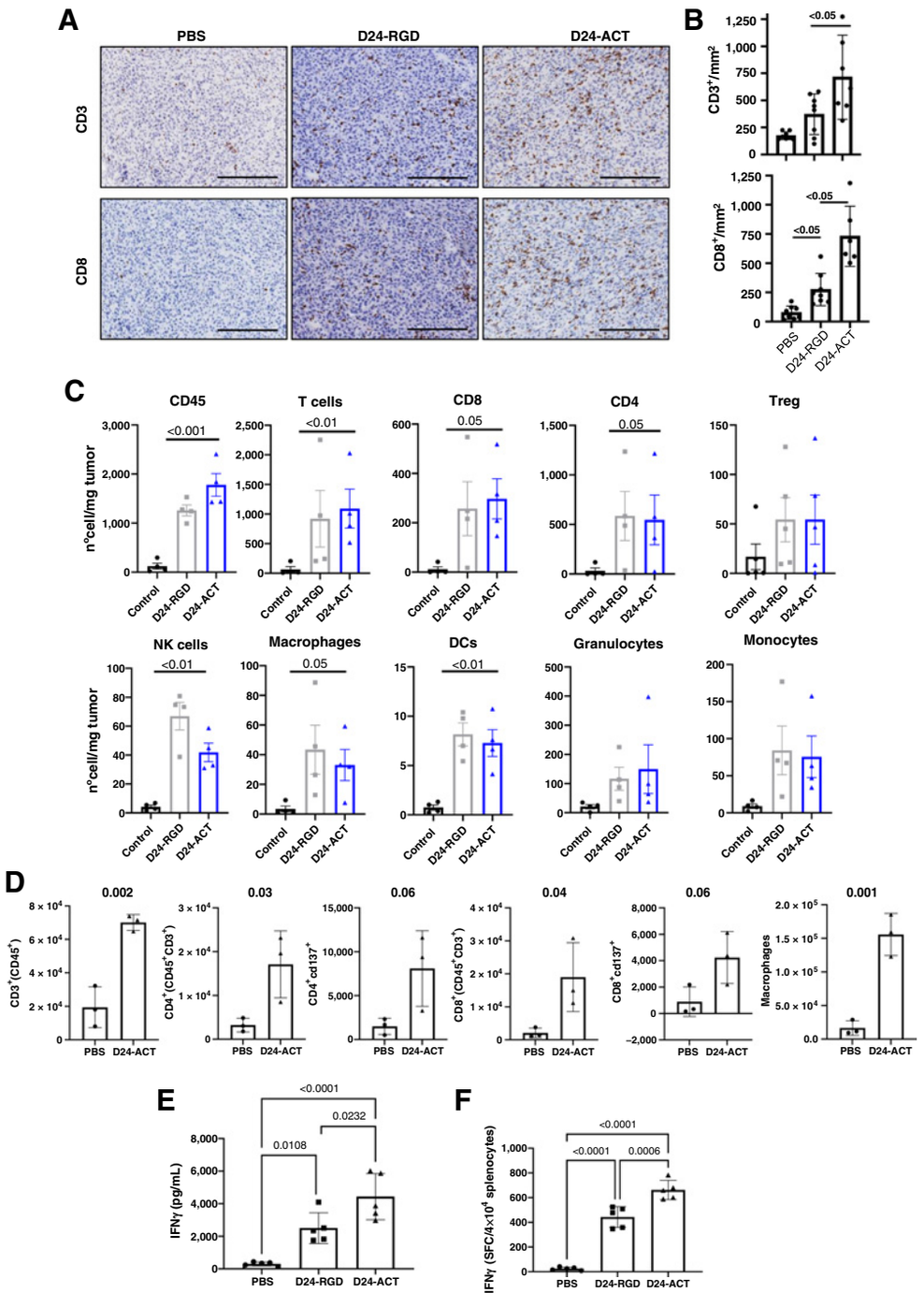

Figure 3.

Administration of Delta-24-ACT results in immune cell infiltration and the production of proinflammatory cytokines. Osteosarcoma tumors were generated by intratibial injection of K7M2 cells, and PBS, Delta-24-RGD, or Delta-24-ACT was administered intratumorally 10 days after cell implantation. Animals were sacrificed on day 17 after cell implantation. **A,** Representative images (scale bar, 100 μm) of CD3 and CD8 immunostaining in osteosarcoma tumors from control mice or virus-treated mice. **B,** Quantification of $CD3^+$ and $CD8^+$ cell infiltration per mm^2 in osteosarcoma tumors ($n = 6–8$). *P* values were calculated using two-tailed Student *t* test. **C,** Flow cytometric analysis of immune cell populations within the TIL population in the tibias of mice bearing intratibial K7M2 tumors and treated with Delta-24-RGD or Delta-24-ACT. The bars indicate the mean ± SD values ($N = 4/5$). **D,** Flow cytometric analysis of immune cell populations within the TIL population in the tibias of mice bearing intratibial K7M2 tumors and treated with Delta-24-ACT. The bars indicate the mean ± SD values ($N = 3$); Mann–Whitney test. **E,** Quantification of IFNγ production by ELISA after 72 hours of coculture of K7M2 cells with splenocytes isolated from mice treated with PBS or the different viruses. The data are presented as the median ± SD values ($n = 5$). One-way ANOVA test was used for comparison between control and treated mice. **F,** Quantification of IFNγ spot-forming cells per 4×10^4 splenocytes isolated from control and Delta-ACT–treated animals and cocultured with tumor cells. *P* values were calculated using one-way ANOVA.

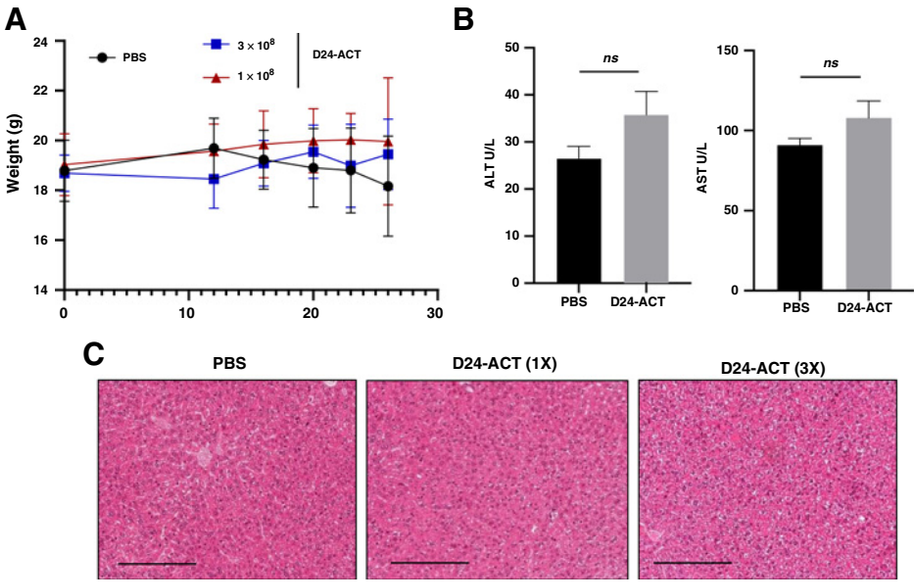

Figure 4.

Administration of Delta-24-ACT presents a safe toxicity profile. **A,** Mice were treated intratibially with mock (PBS) or Delta-24-ACT one or three times at the indicated doses. Mice from the different groups were weighed every 3 to 4 days until the end of the treatment period (25 days). The data are shown as the median ± SD for each group at each time point. **B,** Evaluation of biochemical parameters related to hepatic toxicity after intratumoral injection of Delta-24-ACT. Mice were treated with mock or virus, and serum samples were collected 3 days later. Several parameters, including ALT (U/L) and AST (U/L) levels, were measured to monitor hepatic injury. **C,** Histologic analysis of the livers of mice bearing orthotopic murine osteosarcoma tumors and treated locally with 10^8 PFU Delta-24-ACT one or three times. Representative micrographs of H&E–stained (magnification, 100 μm) livers of mice from the indicated groups are shown. The images show no viral presence in mouse livers and no signs of hepatotoxicity.

Local treatment with Delta-24-ACT increases overall survival in an osteosarcoma murine model

Next, we evaluated the therapeutic effect of the virus. For this study, two local injections were administered on days 10 and 18 (Supplementary Fig. S4A). Mice were weighed until day 40 to rule out toxicity (Supplementary Fig. S4B). Efficacy studies showed that control mice developed visible bone tumors faster than treated mice, and by day 25, all but two control mice exhibited measurable tumors (**Fig. 5A**). Moreover, tumors developed in only four of the 12 tibias in the treated group. The tumor diameters in control mice ranged from 90 to 500 mm^3, whereas the four tumors that developed in the Delta-24-ACT–treated group had volumes between 250 and 450 mm^3 (**Fig. 5A**). Treatment with Delta-24-RGD also delayed tumor growth (Supplementary Fig. S4C). Kaplan–Meier survival curves showed that local administration of Delta-24-ACT led to significantly extended overall survival times, with median survival times of 30 days for PBS-treated mice and 47 days for Delta-24-ACT–treated mice ($P < 0.0001$; **Fig. 5B**). In a second survival study, we compared the efficacy of Delta-24-ACT with Delta-24-RGD and PBS treated mice. We observed that efficacy of Delta-24-ACT was superior to the one exerted by Delta-24-RGD. Kaplan–Meier survival curves showed that local administration of Delta-24-ACT or Delta-24-RGD led to significantly extended overall survival times, with median survival times of 33.5 days for PBS-treated mice, 38 days for Delta-24-RGD ($P < 0.05$) and 60 days for Delta-24-ACT–treated mice ($P = 0.0006$). Both viruses led to the generation of long-term survivors: one (1/10) and four (4/10) for Delta-24-RGD and Delta-24-ACT, respectively (Supplementary Fig. S4D). K7M2 cells are a highly lung metastatic cell line; therefore, we evaluated the potential for lung metastasis. Micro-CT analysis showed that the integrity of the normal lung parenchyma was significantly maintained in mice treated with Delta-24-ACT compared with control mice ($P = 0.05$; **Fig. 5C**), indicating that the viral treatment can control spontaneous lung metastasis. Delta-24-RGD treatment also significantly reduced the number of tumor nodules in the lungs of treated mice (Supplementary Fig. E). Rechallenge of the long-term survivors with K7M2 cells in the contralateral leg showed that 100% of long-term survivors (3/3) were protected against rechallenge through the development of protective immune memory. Moreover, anatomopathological studies showed normal tibias in the animal previously treated with Delta-24-ACT in stark contrast with the tibias of the naïve treated mice (**Fig. 5G**). Lung evaluation also revealed that long-term survivors showed healthier lung parenchyma than naïve counterparts (**Fig. 5H**).

Evaluation of the efficacy of Delta-24-RGD and Delta-24-ACT in immunodeficient model lacking lymphocytes T and B bearing orthotopically K7M2 murine cell line, showed no therapeutic benefit, indicating that the mechanism of action of these viruses is mediated by an efficient antitumoral immune response (**Fig. 5I**; Supplementary Fig. S4F). In summary, these data revealed the efficacy and safety of Delta-24-ACT in a pediatric osteosarcoma murine model.

Discussion

The observation that osteosarcoma tumors exhibit genomic instability and a high mutational burden, associated with an increased presence of neoantigens, suggests that these tumors are amenable to immunotherapy (23). In fact, several immunotherapy-based clinical trials, including trials of immune checkpoint inhibitors, chimeric antigen receptor (CAR) T cells and other immunotherapies (NCT03006848, NCT03628209, NCT04539366, NCT04483778, and

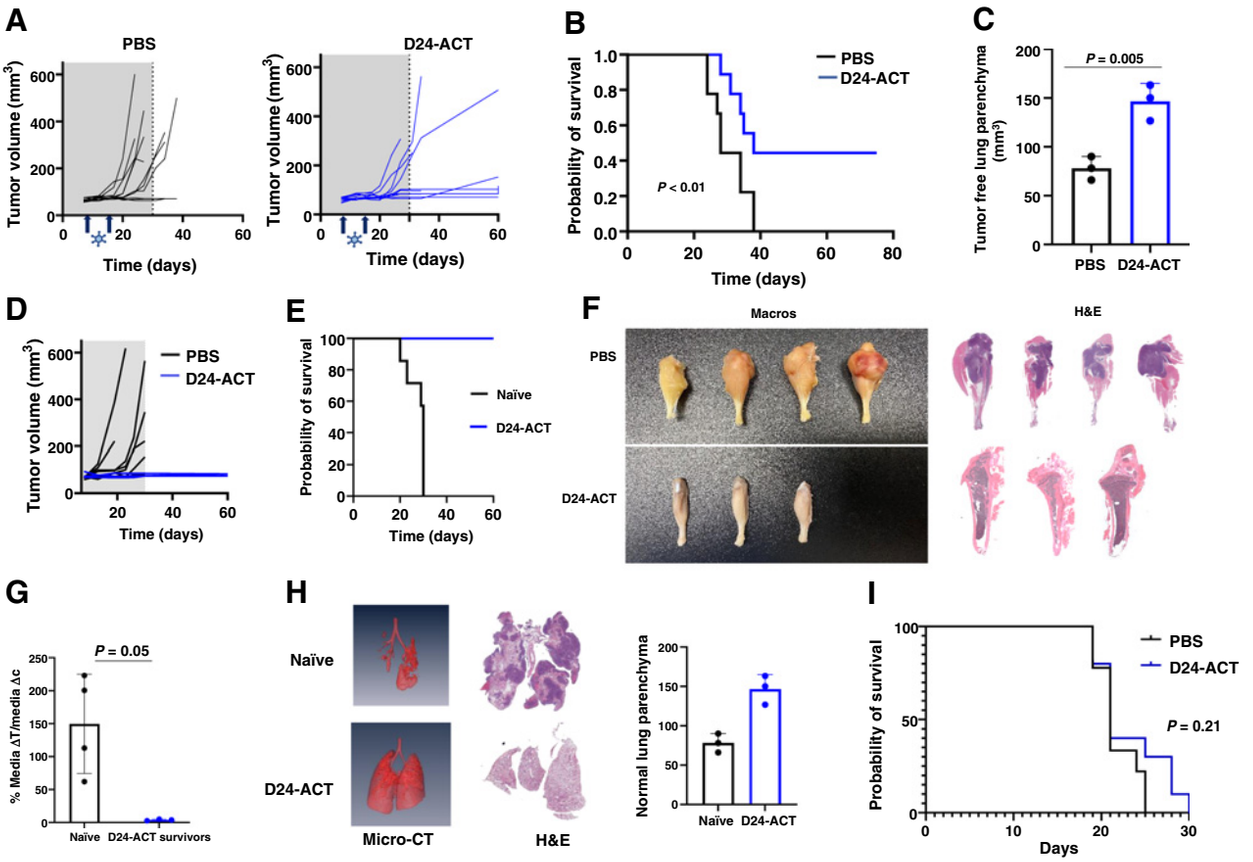

Figure 5.

Administration of Delta-24-ACT results in local and metastatic efficacy effect in a murine osteosarcoma model. **A,** Analyses of tumor burden development in the PBS-treated (control group) and Delta-24-ACT–treated groups. Tumor volume in mouse tibias was measured on different days until the end of the experiment. **B,** Survival curves. The graphs show the overall survival of mice treated with Delta-24-ACT (blue line) or PBS (black line). **C,** Evaluation of lung metastasis using micro-CT. Quantification of the normal lung parenchyma using micro-CT. **D,** The long-term survivors from the Delta-24-ACT–treated group were subjected to rechallenge with K7M2 cells in the contralateral tibia and compared with control untreated mice (naïve). Analyses of tumor burden development in the naïve-treated (control group) and Delta-24-ACT–treated groups. Tumor volume in mouse tibias was measured on different days until the end of the experiment. **E,** Kaplan–Meier survival curves of the long-term survivors from the Delta-24-ACT–treated group subjected to a rechallenge with K7M2 cells in the contralateral tibia and compared with control untreated mice. **F,** Representative macroscopic images and H&E-stained sections of tibias from PBS- or Delta-24-ACT–treated mice. **G,** Differences in tumor growth shown as percentages in comparison with the control groups. **H,** Evaluation of lung metastasis using micro-CT. Representative 3D image reconstruction of the normal lung parenchyma and corresponding histologic macroscopic images of tumors in PBS- and Delta-24-ACT–treated animals (left). Quantification of the normal lung parenchyma using micro-CT (right). **I,** Kaplan–Meier survival curves of Delta-24-ACT (10^7 pfu)-treated and control (PBS)-treated immunodeficient (athymic nude) mice ($n = 11$, both groups) bearing intratibial K7M2 tumors. The *P* value was calculated with the log-rank test.

NCT02470091), are ongoing. However, the published results are modest regarding outcomes in patients with metastatic or refractory osteosarcoma (24, 25). Furthermore, the toxicities induced by some of these agents have hampered their clinical development (26, 27). In this work, we showed that Delta-24-ACT is safe and efficacious in murine osteosarcoma models. Our results are consistent with a plethora of trials that support the inclusion of oncolytic viruses in routine oncology and, most importantly, pediatric oncology (NCT03178032, NTC02444546, NTC03043391, NTC03330197, NTC02031965). Oncolytic viruses have shown good safety profiles and a degree of efficacy (28). These results encourage the combination of these viruses with drugs specifically geared toward targeting aberrancies in pediatric solid tumors. One interesting feature of the virus presented in this work is that the overall survival of the long-term responders (50% of treated mice) developed an effective antiosteosarcoma memory immune response. This capacity of the virus to achieve a "vaccine" effect is of relevance for osteosarcoma therapy because 20% of new cases present with metastasis at diagnosis (29). In this line of thinking, we know that treatment with oncolytic viruses leads to the release of DAMPs and pathogen-associated molecular patterns and ultimately to ICD, which in turn results in tumor antigen release (29). In our system *in vitro*, both viruses led to the release of DAMPs compatible with ICD, and this phenomenon was higher in Delta-24-ACT–treated osteosarcoma cells. Supporting this notion, in an elegant work by Hinterberger and colleagues, where they evaluated the efficacy of a modified Ankara virus (MVA-TAA-4-1BBL) armed with 4-1BBL and administered intratumorally in different tumor models, they observed that the virus triggered profound changes in the tumor microenvironment, including the induction of multiple proinflammatory molecules and ICD (30). However, to clarify the

specific contribution of 4-1BBL to the enhancement of this type of death, further experiments would be needed.

One of the main hurdles of current immunotherapies is the immunosuppressive tumor microenvironment (TME) and the inability to induce a T-cell trafficking to tumor site. Specifically relevant to osteosarcomas is that the presence of malignant osteoid limits immune infiltration into tumor (23). In addition, single-cell RNA sequencing studies of osteosarcoma patient samples have shown that the TME in this type of cancer is highly heterogeneous, with an ample diversity of immune populations with different phenotypes, revealing the complexity of osteosarcoma tumors (30) and suggesting that one strategy does not fit all cancer. We observed that Delta-24-ACT induced T-cell trafficking to osteosarcoma tumors overcoming the immunosuppressive TME. Therefore, the virus could shake the TME and render the tumor more susceptible to other types of immunotherapies such as immune checkpoints. In that line of thinking, an elegant study by Ligon and colleagues uncovered an immune molecular and cellular signature in osteosarcoma pulmonary metastasis that expressed PD-L1, LAG3, and CSF1R and was associated with worse progression-free survival (31). It would be interesting to combine the virus with one or several inhibitors of these molecules and assess the effect on survival.

Besides lymphocytes, we observed a significant upregulation of macrophages in the tumors treated with Delta-24-ACT. Interestingly, this population is prevalent in patients, and their role is complex and context-dependent (32–35). In our work, we did not delve into the phenotype of these cells. In addition, we observed a significant increase in dendritic cells. It is well known that activated APC express high amounts of 4-1BBL. Moreover, it has been shown that immunization with a 4-1BBL lentivirus activates significant numbers of bystander DCs in the draining lymph nodes and leads to more efficacious CD8. In that work, the authors showed that transactivation by 4-1BBL/4-1BB interaction following DC–DC contact could participate in the immune response to infection or vaccination (36). Understanding the potential contribution of APCs to the antisarcoma effect shown by Delta-24-ACT could provide clues to improve this therapy

One limitation of our study is that adenovirus replication is hindered in murine cell lines. The murine osteosarcoma cells used in this work are nonpermissive for adenoviral replication (**Fig. 1**), reducing the adenoviral load and limiting 4-1BBL expression to only a first wave. This constraint probably resulted in milder stimulation of the immune response than that potentially occurring in human counterparts. However, although our study was not ideal, our data showed the efficacy of this virus.

The encouraging results achieved by local administration of Delta-24-ACT, indicating that it can trigger distant tumor remission, underscore the therapeutic potential of this virus and the need for its clinical translation.

Data and materials availability

The data that support the findings of this study are available within the article or Supplementary Information or available from the corresponding author upon request.

Authors' Disclosures

N. Martinez-Velez reports grants from AACR Foundation during the conduct of the study. J. Fueyo reports a patent for Oncolytic adenoviruses pending and licensed to DNAtrix and is a shareholder of DNATrix. C. Gomez-Manzano reports a patent for Oncolytic adenoviruses pending and licensed to DNAtrix and is a shareholder of DNAtrix. M.M. Alonso reports grants from DNAtrix outside the submitted work. No disclosures were reported by the other authors.

Authors' Contributions

N. Martinez-Velez: Conceptualization, methodology, writing–review and editing. **V. Laspidea:** Conceptualization, formal analysis, investigation, methodology, writing–original draft, writing–review and editing. **M. Zalacain:** Conceptualization, investigation, methodology, writing–original draft, writing–review and editing. **S. Labiano:** Investigation, writing–review and editing. **M. Garcia-Moure:** Investigation, writing–review and editing. **M. Puigdelloses:** Investigation, writing–review and editing. **L. Marrodan:** Investigation, writing–review and editing. **M. Gonzalez-Huarriz:** Investigation, writing–review and editing. **G. Herrador:** Investigation, writing–review and editing. **D. de la Nava:** Investigation, writing–review and editing. **I. Ausejo-Mauleon:** Investigation, writing–review and editing. **J. Fueyo:** Formal analysis, methodology, writing–review and editing. **C. Gomez-Manzano:** Formal analysis, methodology, writing–review and editing. **A. Patiño-García:** Conceptualization, resources, funding acquisition, investigation, writing–original draft, writing–review and editing. **M.M. Alonso:** Conceptualization, resources, funding acquisition, investigation, writing–original draft, writing–review and editing.

Acknowledgments

The performed work was supported through the Departamento de Salud del Gobierno de Navarra (54/2018-APG); AACR-AstraZeneca Immuno-oncology Research Fellowship (18-40-12-MART; N. Martinez-Velez); Predoctoral Fellowship from Gobierno de Navarra (V. Laspidea and G. Herrador), Instituto de Salud Carlos III y Fondos Feder (PI19/01896 M.M. Alonso, PI18/00164A. Patiño-García); Amigos de la Universidad de Navarra (to M. Puigdelloses); Fundación La Caixa/Caja Navarra (A. Patiño-García and M.M. Alonso); Fundación El Sueño de Vicky; Asociación Pablo Ugarte-Fuerza Julen, Fundación ADEY, Fundación ACS, (A. Patiño-García and M.M. Alonso); and Department of Defense (DOD) Team Science Award under grant (CA 160525 M.M. Alonso, C. Gomez-Manzano, and J. Fueyo). La Marató (M.M. Alonso). This project also received funding from the European Research Council (ERC) under the European Union's Horizon 2020 Research and Innovation Programme (817884 ViroPedTher to M.M. Alonso).

The costs of publication of this article were defrayed in part by the payment of page charges. This article must therefore be hereby marked *advertisement* in accordance with 18 U.S.C. Section 1734 solely to indicate this fact.

Received June 29, 2021; revised October 26, 2021; accepted December 15, 2021; published first December 29, 2021.

References

1. Mirabello L, Troisi RJ, Savage SA. Osteosarcoma incidence and survival rates from 1973 to 2004: Data from the surveillance, epidemiology, and end results program. Cancer 2009;115:1531–43.
2. Morrow JJ, Khanna C. Osteosarcoma genetics and epigenetics: Emerging biology and candidate therapies. Crit Rev Oncog 2015;20:173–97.
3. Chou AJ, Gorlick R. Chemotherapy resistance in osteosarcoma: current challenges and future directions. Expert Rev Anticancer Ther 2006;6:1075–85.
4. Fueyo J, Alemany R, Gomez-Manzano C, Fuller GN, Khan A, Conrad CA, et al. Preclinical characterization of the antiglioma activity of a tropism-enhanced adenovirus targeted to the retinoblastoma pathway. J Natl Cancer Inst 2003;95:652–60.
5. Suzuki K, Alemany R, Yamamoto M, Curie DT. The presence of the adenovirus E3 region improves the oncolytic potency of conditionally replicative adenoviruses. Clin Cancer Res 2002;8:3348–59.
6. Alonso MM, Gomez-Manzano C, Bekele BN, Yung WKA, Fueyo J. Adenovirus-based strategies overcome temozolomide resistance by silencing the O6-methylguanine-DNA methyltransferase promoter. Cancer Res 2007;67:11499–504.
7. Martínez-Vélez N, Garcia-Moure M, Marigil M, González-Huarriz M, Puigdelloses M, Gallego Pérez-Larraya J, et al. The oncolytic virus Delta-24-RGD elicits an antitumor effect in pediatric glioma and DIPG mouse models. Nat Commun 2019;10:2235.

8. Martinez-Velez N, Xipell E, Jauregui P, Zalacain M, Marrodan L, Zandueta C, et al. The oncolytic adenovirus Δ24-RGD in combination with cisplatin exerts a potent anti-osteosarcoma activity. J Bone Miner Res 2014;29:2287–96.
9. Garcia-Moure M, Gonzalez-Huarriz M, Labiano S, Guruceaga E, Bandres E, Zalacain M, et al. Delta-24-RGD, an oncolytic adenovirus, increases survival and promotes proinflammatory immune landscape remodeling in models of AT/RT and CNS-PNET. Clin Cancer Res 2021;27:1807–20.
10. Lang FF, Conrad C, Gomez-Manzano C, Alfred Yung WK, Sawaya R, Weinberg JS, et al. Phase I study of DNX-2401 (delta-24-RGD) oncolytic adenovirus: replication and immunotherapeutic effects in recurrent malignant glioma. J Clin Oncol 2018; 36:1419–27.
11. Cheuk ATC, Mufti GJ, Guinn BA. Role of 4–1BB:4–1BB ligand in cancer immunotherapy. Cancer Gene Ther 2004;11:215–26.
12. Chester C, Sanmamed MF, Wang J, Melero I. Immunotherapy targeting 4-1BB: Mechanistic rationale, clinical results, and future strategies. Blood 2018; 131:49–57.
13. Kamijo A, Koshino T, Uesugi M, Nitto H, Sai T. Inhibition of lung metastasis of osteosarcoma cell line POS-1 transplanted into mice by thigh ligation. Cancer Lett 2002;188:213–9.
14. Joliat MJ, Umeda S, Lyons BL, Lynes MA, Shultz LD. Establishment and characterization of a new osteogenic cell line (MOS-J) from a spontaneous C57BL/6J mouse osteosarcoma. In Vivo 2002;16:223–8.
15. Puigdelloses M, Garcia-Moure M, Labiano S, Laspidea V, Gonzalez-Huarriz M, Zalacain M, et al. CD137 and PD-L1 targeting with immunovirotherapy induces a potent and durable antitumor immune response in glioblastoma models. J Immunother Cancer 2021;9:e002644.
16. Martínez-Vélez N, Xipell E, Vera B, De La Rocha AA, Zalacain M, Marrodan L, et al. The oncolytic adenovirus VCN-01 as therapeutic approach against pediatric osteosarcoma. Clin Cancer Res 2016;22:2217–25.
17. Kroemer G, Galluzzi L, Kepp O, Zitvogel L. Immunogenic cell death in cancer therapy. Annu Rev Immunol 2013;31:51–72.
18. Garg AD, Nowis D, Golab J, Vandenabeele P, Krysko DV, Agostinis P. Immunogenic cell death, DAMPs and anticancer therapeutics: An emerging amalgamation. Biochim Biophys Acta 2010;1805:53–71.
19. Lin SY, Hsieh SY, Fan YT, Wei WC, Hsiao PW, Tsai DH, et al. Necroptosis promotes autophagy-dependent upregulation of DAMP and results in immunosurveillance. Autophagy 2018;14:778–95.
20. Thorburn J, Horita H, Redzic J, Hansen K, Frankel AE, Thorburn A. Autophagy regulates selective HMGB1 release in tumor cells that are destined to die. Cell Death Differ 2009;16:175–83.
21. Jiang H, Clise-Dwyer K, Ruisaard KE, Fan X, Tian W, Gumin J, et al. Delta-24-RGD oncolytic adenovirus elicits anti-glioma immunity in an immunocompetent mouse model. PLoS One 2014;9:e97407.
22. Sanmamed MF, Pastor F, Rodriguez A, Perez-Gracia JL, Rodriguez-Ruiz ME, Jure-Kunkel M, et al. Agonists of co-stimulation in cancer immunorapy directed against CD137, OX40, GITR, CD27, CD28, and ICOS. Semin Oncol 2015;42: 640–55.
23. Wu CC, Beird HC, Andrew Livingston J, Advani S, Mitra A, Cao S, et al. Immuno-genomic landscape of osteosarcoma. Nat Commun 2020;11:1008.
24. Boye K, Longhi A, Guren T, Lorenz S, Næss S, Pierini M, et al. Pembrolizumab in advanced osteosarcoma: results of a single-arm, open-label, phase 2 trial. Cancer Immunol Immunother 2021;70:2617–24.
25. DeRenzo C, Gottschalk S. Genetically modified T-cell therapy for osteosarcoma: into the roaring 2020s. Adv Exp Med Biol 2020;1257:109–31.
26. Boutros C, Tarhini A, Routier E, Lambotte O, Ladurie FL, Carbonnel F, et al. Safety profiles of anti-CTLA-4 and anti-PD-1 antibodies alone and in combination. Nat Rev Clin Oncol 2016;13:473–86.
27. Gust J, Hay KA, Hanafi LA, Li D, Myerson D, Gonzalez-Cuyar LF, et al. Endothelial activation and blood–brain barrier disruption in neurotoxicity after adoptive immunotherapy with CD19 CAR-T cells. Cancer Discov 2017; 7:1404–19.
28. Martinez-Quintanilla J, Seah I, Chua M, Shah K. Oncolytic viruses: overcoming translational challenges. J Clin Invest 2019;29:1407–18.
29. Moore DD, Luu HH. Osteosarcoma. Cancer Treat Res 2014;162:65–92.
30. Zhou Y, Yang D, Yang Q, Lv X, Huang W, Zhou Z, et al. Single-cell RNA landscape of intratumoral heterogeneity and immunosuppressive microenvironment in advanced osteosarcoma. Nat Commun 2020;11:6322.
31. Ligon JA, Choi W, Cojocaru G, Fu W, Hsiue EH-C, Oke TF, et al. Pathways of immune exclusion in metastatic osteosarcoma are associated with inferior patient outcomes. J Immunother Cancer 2021;9:e001772.
32. Toulmonde M, Penel N, Adam J, Chevreau C, Blay JY, Le Cesne A, et al. Use of PD-1 targeting, macrophage infiltration, and IDO pathway activation in sarcomas a phase 2 clinical trial. JAMA Oncol 2018;4:93–7.
33. Shiraishi D, Fujiwara Y, Horlad H, Saito Y, Iriki T, Tsuboki J, et al. CD163 is required for protumoral activation of macrophages in human and murine sarcoma. Cancer Res 2018;78:3255–66.
34. Buddingh EP, Kuijjer ML, Duim RAJ, Bürger H, Agelopoulos K, Myklebost O, et al. Tumor-infiltrating macrophages are associated with metastasis suppression in high-grade osteosarcoma: a rationale for treatment with macrophage activating agents. Clin Cancer Res 2011;17:2010–19.
35. Heymann MF, Lézot F, Heymann D. The contribution of immune infiltrates and the local microenvironment in the pathogenesis of osteosarcoma. Cell Immunol 2019;343:103711.
36. Macdonald DC, Hotblack A, Akbar S, Britton G, Collins MK. 4–1BB ligand activates bystander dendritic cells to enhance immunization in trans. J Immunol 2014;193:5056–64.